Optimal Frequency Control with Operational Constraints: An Enhanced Distributed Averaging-Based Integral Approach

Yixuan Yu, Yan Jiang, and Pengcheng You

Abstract— **Frequency control is essential for the stable operation of power systems. Compared to traditional integral controllers, the distributed averaging-based integral (DAI) controller achieves frequency restoration and optimal steady state simultaneously through local frequency sensing and neighbor communication. However, the standard DAI controller does not guarantee the satisfaction of operational constraints. In this paper, we reinterpret the DAI controller from a primal-dual perspective and propose a projection-based improvement that enforces these constraints. The enhanced controller ensures that generator outputs remain within power rating constraints throughout the entire process, even during the transient, and that line power flows satisfy thermal limits at steady state. We establish the asymptotic convergence of the enhanced DAI controller using a Lyapunov function based on Clarke generalized gradient. Simulation results demonstrate that the proposed controller not only stabilizes the power system and restores the nominal frequency, but also maintains compliance with operational constraints.**

I. Introduction

The stability of power systems typically requires that the frequency remains at its nominal value (50 Hz or 60 Hz) in real time, in order to ensure the safe and reliable operation of equipment within the grid. When there is an imbalance between supply and demand, frequency deviation occurs, necessitating the design of controllers to restore and stabilize the frequency as quickly as possible. Traditionally, from a time-scale perspective, frequency control is divided into three stages: primary control for stabilizing the frequency, secondary control for restoring the frequency to its nominal value, and tertiary control for optimizing the economic performance of the power system.

There are numerous studies aiming at secondary frequency control, many of which adopt centralized approaches. With the increasing integration of diverse energy sources and the growing scale of power grids, centralized control approaches face challenges in achieving fast and accurate regulation. Therefore, distributed control strategies are increasingly favored, as they reduce computational complexity while improving both control efficiency and economic performance of the power system.

Various distributed control algorithms [1]–[7] has been adopted to simultaneously achieve frequency restoration and optimal steady state. In [1], the linear distributed averaging-based integral (DAI) controller was first proposed. Building upon the concept of integral control, the authors incorporated the marginal cost differences between neighboring nodes into the integrator to enhance economic efficiency. While the DAI controller effectively regulates frequency and ensures an optimal steady state, it does not explicitly account for operational constraints such as power rating limits and line thermal limits, as these constraints are not inherently incorporated into its control structure.

A natural approach to incorporating constraints is to formulate the control objective as a constrained optimization problem, allowing for the search for feasible and optimal solutions. Extensive studies have reformulated the frequency control problem as a constrained optimization task, enabling controller design through primal-dual algorithmic frameworks. For example, [8] interprets automatic generation control (AGC) from an optimization perspective, allowing improvements in its economic efficiency. In [9], [10], element-wise projection for line thermal limits is incorporated into the controller, and its validity and convergence are rigorously established through the primal-dual algorithm. In [11], both power rating constraints and line thermal limits are incorporated into the controller through distinct projection operators.

In this paper, we focus on how to reverse engineer the DAI controller using primal-dual principles and then incorporate operational constraints into the controller design via an optimization formulation. We first formulate an optimization problem equivalent to the original control problem while explicitly incorporating operational constraints. By leveraging this formulation, we interpret the closed-loop system's trajectory as an iterative process for searching the optimal solution of the optimization problem. Then, according to primal-dual algorithm, we incorporate projection operators with distinct functionalities into the controller to enforce two kinds of operational constraints. Furthermore, we characterize the system's equilibrium points based on the established equivalence between the optimization and control problems. Finally, we validate the proposed controller through simulations that demonstrate its ability to ensure stability and enforce operational constraints compared to the original DAI controller.

Our contributions are summarized as follows.

1) We reinterpret the linear DAI controller from a primal-dual perspective and formulate an constrained optimization problem to enhance its design, ensuring compliance with operational constraints.
2) By leveraging the primal-dual algorithm, we design a controller with projection operators, which is proven to asymptotically stabilize the system and ensure conver-

Y. Yu and P. You are with the College of Engineering, Peking University, Beijing, China yuyixuan834@stu.pku.edu.cn, pcyou@pku.edu.cn

Y. Jiang is with the School of Science and Engineering, The Chinese University of Hong Kong, Shenzhen, Shenzhen, China yjiang@cuhk.edu.cn

gence to the nominal frequency value using a Clarke-gradient-based Lyapunov function.
3) Numerical results validate the convergence of the proposed controller. Furthermore, the power rating constraints are strictly enforced even during the transient, while the line thermal limits are enforced at steady state.

Notations. Throughout this paper, vectors are all column vectors by default and denoted by lower-case letters in bold while matrices are denoted by upper-case letters in bold. Besides, $\mathbb{1}_n \in \mathbb{R}^n$ and $\mathbb{0}_n \in \mathbb{R}^n$ denote the vectors of all ones and all zeros, respectively.

II. Problem Statement

We consider an n-bus power network with the topology characterized by a directed and connected graph $(\mathcal{V}, \mathcal{E})$, where the buses indexed by $i \in \mathcal{V} := \{1, \dots, n\}$ are connected through the transmission lines indexed by ordered pairs $(i,j) \in \mathcal{E} \subset \mathcal{V} \times \mathcal{V}$. Without loss of generality, we assume there is only one aggregate controllable generator at each bus subject to a linear approximation of swing dynamics [12]. More precisely, given the power disturbance p_i at bus $i \in \mathcal{V}$, represented by a step change scalar, the dynamics of the phase angle θ_i and the frequency ω_i from the nominal frequency are given by

$$\dot{\theta}_i = \omega_i \,, \tag{1a}$$

$$m_i \dot{\omega}_i = -\alpha_i \omega_i - \sum_{j=1}^{n} B_{ij} \left(\theta_i - \theta_j\right) - p_i + u_i \,, \tag{1b}$$

where $m_i > 0$ is the generator inertia constant, $\alpha_i > 0$ summarizes the generator damping and frequency-dependent load, and $B_{ij} > 0$ characterizes the sensitivity of the power flow on line (i,j) to the phase angle differences between its two end buses, if $(i,j) \in \mathcal{E}$. u_i is a controllable power injection, by generator, to be designed for frequency control. Note that the linearized network model (1) implicitly assumes that the variables θ_i, ω_i, u_i as well as the parameter p_i are deviations from their nominal values.

The basic goal of secondary frequency control for the power system is to not only stabilize the frequencies $\boldsymbol{\omega} := (\omega_i, i \in \mathcal{V}) \in \mathbb{R}^n$, i.e., $\dot{\boldsymbol{\omega}} = \mathbb{0}_n$ but also restore them to the nominal value $\boldsymbol{\omega} = \mathbb{0}_n$. We further require that at the steady state, the control efforts have to be optimally allocated according to, for instance, a given quadratic cost function $f_i(u_i) := \frac{1}{2} c_i u_i^2$ for the power injection at each bus i, where $c_i > 0$ is constant cost coefficient. Meanwhile, (1b) reduces to a characterization of the nodal power balance over the network:

$$u_i - p_i - \sum_{j=1}^{n} B_{ij}(\theta_i - \theta_j) = 0 \,, \qquad \forall i \in \mathcal{V} \,. \tag{2}$$

The power flow on each line (i,j) cannot exceed the allowable thermal limits $\underline{P}_{ij}$ and $\overline{P}_{ij}$, i.e.,

$$\underline{P}_{ij} \le P_{ij} = B_{ij}(\theta_i - \theta_j) \le \overline{P}_{ij} \,, \qquad \forall (i,j) \in \mathcal{E} \,. \tag{3}$$

Moreover, the controllable power output at each bus i is often constrained by the physical capacity $\overline{u}_i$ and the potential minimum output $\underline{u}_i$, i.e.,

$$\underline{u}_i \le u_i \le \overline{u}_i \,, \qquad \forall i \in \mathcal{V} \,. \tag{4}$$

Therefore, given $\boldsymbol{p} := (p_i, i \in \mathcal{V}) \in \mathbb{R}^n$, the optimal steady-state problem that minimizes the aggregate control cost to maintain the network power balance subject to the physical constraints is given by

$$\begin{aligned} \underset{\boldsymbol{u}}{\text{minimize}} \quad & f(\boldsymbol{u}) := \sum_{i=1}^{n} f_i(u_i) \\ \text{subject to} \quad & \text{(2)(3)(4)} \end{aligned} \tag{5}$$

with the control input $\boldsymbol{u} := (u_i, i \in \mathcal{V}) \in \mathbb{R}^n$.

In addition to the steady-state requirements characterized by (2)(3)(4), another important practical factor to be taken into account is that the power rating constraint (4) has to be always respected, even during the transient. Due to such a characteristic, the two types of operational constraints (3) and (4) are fundamentally different. Put together, the goal of the optimal frequency control with the operational constraints is to design a controller $\boldsymbol{u}$, subject to the transient constraint (4), to simultaneously realize the frequency stabilization and restoration as well as the optimal steady state described by the optimization problem (5). We assume such a controller exists with proper given parameters, which is a standing assumption of this work.

III. DAI Control Revisited

While the literature on secondary frequency control is huge, there has been little existing work that accounts for the operational constraints during the transient while meeting the steady-state requirements. We will particularly work with an emerging DAI control structure and show how it could be enhanced to achieve our control goal. We first revisit the DAI control in this section to analyze its performance bottleneck.

The DAI control is a distributed control strategy rooted in the conventional integral control. It incorporates distributed communication and averaging mechanisms to enable system-wide consensus on both frequencies at the nominal value and marginal control costs, a common sign of efficient allocation [13]. Specifically, in our setting the controller $\boldsymbol{u}$ will consist of two corresponding integrals as follows: $\forall i \in \mathcal{V}$,

$$u_i = k_i \xi_i \,, \tag{6a}$$

$$\dot{\xi}_i = -\omega_i - c_i \sum_{j=1}^{n} Q_{ij}(c_i u_i - c_j u_j) \,. \tag{6b}$$

Here $k_i > 0$ is a control gain. Q_{ij} is a weight on line (i,j) with $Q_{ij} = Q_{ji} > 0$ if buses i and j are adjacent and $Q_{ij} = Q_{ji} = 0$, otherwise. It leads to a matrix $\boldsymbol{Q}$ with Q_{ij} being the $(i,j)^{\text{th}}$ entry. $c_i u_i$ is the derivative of the cost function $f_i(u_i)$, i.e., the marginal cost of the control input u_i. $\boldsymbol{\xi} := (\xi_i, i \in \mathcal{V})$ is thus the integral of the sum of local frequency deviation and marginal cost differences between neighboring nodes, which serves to eliminate frequency deviation and drive identical marginal costs at equilibrium.

Given $\boldsymbol{\theta} := (\theta_i, i \in \mathcal{V}) \in \mathbb{R}^n$ and $\boldsymbol{B} := \text{diag}(B_{ij}, (i,j) \in \mathcal{E}) \in \mathbb{R}^{|\mathcal{E}|\times|\mathcal{E}|}$, the closed-loop system (1), (6) admits a set of equilibria that are asymptotically stable, as described below.

Lemma 1 (Theorem 3 [13]): For the closed-loop system (1), (6), a point $(\boldsymbol{\theta}^*, \boldsymbol{\omega}^*, \boldsymbol{u}^*)$ is an equilibrium if and only if it satisfies

$$\boldsymbol{\omega}^* = \mathbb{0}_n\,, \tag{7a}$$
$$\boldsymbol{B}\boldsymbol{C}^T\boldsymbol{\theta}^* = \boldsymbol{u}^* - \boldsymbol{p}\,, \tag{7b}$$
$$\boldsymbol{u}^* = \pi\boldsymbol{\Xi}^{-1}\mathbb{1}_n\,, \tag{7c}$$

where $\boldsymbol{C}$ is the incidence matrix of the network $(\mathcal{V}, \mathcal{E})$, $\boldsymbol{\Xi} := \text{diag}(c_i, i \in \mathcal{V})$ is a diagonal matrix of all cost coefficients, and $\pi := \sum_{i\in\mathcal{V}} p_i / \sum_{i\in\mathcal{V}} c_i^{-1}$ is a constant. Furthermore, the set of equilibria are asymptotically stable.

Lemma 1 reveals that the canonical DAI control is able to achieve secondary frequency control with certain steady-state performance guarantees. Notably, π relates to the notion of shadow price in economics, and thus (7c) implies the optimality condition of the following problem:

$$\begin{aligned} \underset{\boldsymbol{u}}{\text{minimize}} \quad & f(\boldsymbol{u}) = \sum_{i=1}^{n} f_i(u_i) \\ \text{subject to} \quad & (2) \end{aligned} \tag{8}$$

Obviously, while the DAI control (6) is aware of efficient allocation of control efforts via the consensus of marginal costs, it does not take into account the transient and equilibrium operational constraints (3), (4). Meanwhile, in the presence of these constraints, the optimum might also be shifted. It remains a core challenge whether the DAI control, even with the constraints accounted for, can still achieve the optimal steady state while stabilizing and restoring the frequencies.

IV. Enhanced DAI Control

To incorporate the operational constraints, we are inspired by primal-dual dynamics that embed the optimizers of an optimization problem in the equilibrium set, and use the idea to develop a novel interpretation for the DAI control. On this basis, we can further employ projection techniques for primal-dual dynamics to enchance the DAI controller and handle the two types of operational constraints.

A. Interpretation as Primal-Dual Dynamics

A key enabler for the primal-dual dynamics interpretation of the DAI control (6) is an underlying optimization problem that reflects both the equilibrium properties and the transient dynamics [9], [14]. We propose the following novel formulation in terms of the closed-loop system (1), (6):

$$\underset{\boldsymbol{\theta},\boldsymbol{\omega},\boldsymbol{u}}{\text{minimize}} \quad \frac{1}{2}\boldsymbol{\omega}^T\boldsymbol{A}\boldsymbol{\omega} + \frac{1}{2}\boldsymbol{u}^T\boldsymbol{\Xi}\boldsymbol{L}_Q\boldsymbol{\Xi}\boldsymbol{u} \tag{9a}$$
$$\text{subject to} \quad \boldsymbol{u} - \boldsymbol{p} - \boldsymbol{A}\boldsymbol{\omega} = \boldsymbol{C}\boldsymbol{B}\boldsymbol{C}^T\boldsymbol{\theta} \tag{9b}$$

with $\boldsymbol{A} = \text{diag}(\alpha_i, i \in \mathcal{V})$, $\boldsymbol{L}_{Q,ij} = -Q_{ij}$ if $i \neq j$ and $\boldsymbol{L}_{Q,ij} = \sum_{l=1,l\neq i}^{n} Q_{il}$ if $i = j$. Cost function (9a) is consists of two convex functions with respect to $\boldsymbol{\omega}$ and $\boldsymbol{u}$ respectively and equality constraint (9b) is consistent with $\dot{\omega}_i = 0$ in (1b) at steady state. Optimization problem (9) is designed such that the controller derived from its primal-dual dynamics aligns with the DAI controller (6). The closed-loop system (1), (6) is actually equivalent to solving (9) with primal-dual algorithm.

To solve (9), according to primal-dual algorithm, we first present the following Lagrangian function:

$$\begin{aligned} L_1 = \frac{1}{2}\boldsymbol{\omega}^T\boldsymbol{A}\boldsymbol{\omega} + \frac{1}{2}\boldsymbol{u}^T\boldsymbol{\Xi}\boldsymbol{L}_Q\boldsymbol{\Xi}\boldsymbol{u} \\ + \boldsymbol{\nu}^T\left(\boldsymbol{u} - \boldsymbol{p} - \boldsymbol{A}\boldsymbol{\omega} - \boldsymbol{C}\boldsymbol{B}\boldsymbol{C}^T\boldsymbol{\theta}\right)\,, \end{aligned} \tag{10}$$

where $\boldsymbol{\nu} := (\nu_i, i \in \mathcal{V})$ is Lagrangian multiplier for (9b).

Before implementing primal-dual algorithm, we first clarify that $\boldsymbol{\nu}(t) \equiv \boldsymbol{\omega}(t)$. As similarly interpreted in [9], [10], we define a reduced Lagrangian function with respect to $(\boldsymbol{\theta}, \boldsymbol{u}, \boldsymbol{\nu})$

$$\hat{L}_1(\boldsymbol{\theta}, \boldsymbol{u}, \boldsymbol{\nu}) = \underset{\boldsymbol{\omega}}{\text{minimize}}\ L_1(\boldsymbol{\theta}, \boldsymbol{u}, \boldsymbol{\omega}, \boldsymbol{\nu})\,. \tag{11}$$

The gradient of $\hat{L}_1$ with respect to $\boldsymbol{\nu}$ is

$$\frac{\partial}{\partial\boldsymbol{\nu}}\hat{L}_1 = \boldsymbol{u} - \boldsymbol{p} - \boldsymbol{A}\boldsymbol{\nu} - \boldsymbol{C}\boldsymbol{B}\boldsymbol{C}^T\boldsymbol{\theta}\,. \tag{12}$$

According to the primal-dual algorithm, variables are updated via gradient flow. Thus, the update for $\boldsymbol{\nu}$ is given by:

$$\dot{\boldsymbol{\nu}} = \boldsymbol{M}^{-1}\left(\boldsymbol{u} - \boldsymbol{p} - \boldsymbol{A}\boldsymbol{\nu} - \boldsymbol{C}\boldsymbol{B}\boldsymbol{C}^T\boldsymbol{\theta}\right)\,, \tag{13}$$

which shares the same dynamics with $\boldsymbol{\omega}$ in (1) with positive stepsizes $\frac{1}{m_i}$. Hence we have $\boldsymbol{\nu}(t) \equiv \boldsymbol{\omega}(t)$ as long as $\boldsymbol{\nu}(0) = \boldsymbol{\omega}(0)$. Therefore, in the subsequent controller design process, we can always replace $\boldsymbol{\nu}$ with $\boldsymbol{\omega}$.

According to the gradient flow of the Lagrangian function (10), variables $(\boldsymbol{\theta}, \boldsymbol{\omega}, \boldsymbol{\xi})$ updates as follows:

$$\dot{\boldsymbol{\theta}} = \boldsymbol{\omega} \tag{14a}$$
$$\dot{\boldsymbol{\omega}} = \boldsymbol{M}^{-1}(\boldsymbol{u} - \boldsymbol{p} - \boldsymbol{A}\boldsymbol{\omega} - \boldsymbol{C}\boldsymbol{B}\boldsymbol{C}^T\boldsymbol{\theta}) \tag{14b}$$
$$\dot{\boldsymbol{\xi}} = -\boldsymbol{K}(\boldsymbol{\omega} + \boldsymbol{\Xi}\boldsymbol{L}_Q\boldsymbol{\Xi}\boldsymbol{u}) \tag{14c}$$

where $\boldsymbol{K} = \text{diag}(k_i, i \in \mathcal{V})$ is the diagonal control gain matrix and $\boldsymbol{u} = \boldsymbol{K}\boldsymbol{\xi}$. Up to a constant coefficient matrix $\boldsymbol{K}$, closed-loop system (14) shares the same structural form as the DAI-controller-based closed-loop system (1), (6). Thus, the controller (14c) reinterprets the DAI controller (6) from the perspective of the primal-dual algorithm.

B. Redesign to Accommodate Operational Constraints

After interpreting the DAI controller with the primal-dual dynamics, we modify it, from the perspective of optimization, to ensure that the system respects power rating constraint and line thermal limits while restoring frequency to nominal value.

- *Power Rating Constraint:* Each generator is subject to power rating constraint, which are expected to be satisfied even during the transient state. Inspired by [14], we employ the following element-wise projection operator

$$[u_i]_{\underline{u}_i}^{\overline{u}_i} := \begin{cases} \overline{u}_i & \text{if } u_i > \overline{u}_i\,, \\ u_i & \text{if } \underline{u}_i \le u_i \le \overline{u}_i\,, \\ \underline{u}_i & \text{if } u_i < \underline{u}_i\,, \end{cases} \tag{15}$$

and the vector case $[\boldsymbol{u}]_{\underline{\boldsymbol{u}}}^{\overline{\boldsymbol{u}}}$ is defined accordingly. Then we incorporate the projection operator into controller (14c) and have

$$\dot{\boldsymbol{\theta}} = \boldsymbol{\omega} \tag{16a}$$

$$\dot{\boldsymbol{\omega}} = \boldsymbol{M}^{-1}(\boldsymbol{u} - \boldsymbol{p} - \boldsymbol{A}\boldsymbol{\omega} - \boldsymbol{C}\boldsymbol{B}\boldsymbol{C}^T\boldsymbol{\theta}) \tag{16b}$$

$$\dot{\boldsymbol{\xi}} = \boldsymbol{K}^{-1}\left[\boldsymbol{K}\boldsymbol{\xi} - \boldsymbol{\omega} - \boldsymbol{\Xi}\boldsymbol{L}_Q\boldsymbol{\Xi}\boldsymbol{u}\right]_{\underline{\boldsymbol{u}}}^{\overline{\boldsymbol{u}}} - \boldsymbol{\xi} \tag{16c}$$

Here, (16c) ensures that the power rating constraint (4) is always satisfied throughout the trajectory without compromising system stability or steady-state performance, which will be proved after we finish the entire controller design.

- *Line Thermal Limits:* In addition to power rating constraints, line thermal limits (3) are also of concern. Unlike the former, momentary violations of power flow limits on transmission lines are acceptable. Therefore, we consider incorporating (3) as constraints in an optimization problem to enforce it in steady state.

Thus, we consider another optimization problem other than (9) to achieve our goal of enhancing DAI controller that respects operational constraints (3) and (4) simultaneously. That is

$$\underset{\boldsymbol{\theta},\boldsymbol{\omega},\boldsymbol{u},\boldsymbol{\phi}}{\text{minimize}} \quad \frac{1}{2}\boldsymbol{\omega}^T\boldsymbol{A}\boldsymbol{\omega} + \frac{1}{2}\boldsymbol{u}^T\boldsymbol{\Xi}\boldsymbol{L}_Q\boldsymbol{\Xi}\boldsymbol{u} \tag{17a}$$

$$\text{subject to} \quad \boldsymbol{u} - \boldsymbol{p} - \boldsymbol{A}\boldsymbol{\omega} = \boldsymbol{C}\boldsymbol{B}\boldsymbol{C}^T\boldsymbol{\theta} \quad : \boldsymbol{\nu} \tag{17b}$$

$$\boldsymbol{u} - \boldsymbol{p} = \boldsymbol{C}\boldsymbol{B}\boldsymbol{C}^T\boldsymbol{\phi} \quad : \boldsymbol{\lambda} \tag{17c}$$

$$\boldsymbol{C}^T\boldsymbol{\phi} \le \overline{\boldsymbol{\theta}} \quad : \boldsymbol{\eta}^+ \tag{17d}$$

$$\underline{\boldsymbol{\theta}} \le \boldsymbol{C}^T\boldsymbol{\phi} \quad : \boldsymbol{\eta}^- \tag{17e}$$

$$\underline{\boldsymbol{u}} \le \boldsymbol{u} \le \overline{\boldsymbol{u}} \tag{17f}$$

where, following [9], we use virtual flows to incorporate (2) as (17c), (3) as (17d)(17e), and (4) as (17f), respectively, with $\boldsymbol{\phi} := (\phi_i, i \in \mathcal{V})$ being virtual phase angle that substitutes $\boldsymbol{\theta}$ and $\boldsymbol{B}\boldsymbol{C}^T\boldsymbol{\phi}$ being the so-called virtual flow. We now illustrate the relationship between the phase angle $\boldsymbol{\theta}$ and virtual phase $\boldsymbol{\phi}$ as the following lemma.

Lemma 2: If $(\boldsymbol{\theta}^\star, \boldsymbol{\omega}^\star, \boldsymbol{u}^\star, \boldsymbol{\phi}^\star)$ is the optimal solution of (17), then $\boldsymbol{C}^T\boldsymbol{\theta}^\star = \boldsymbol{C}^T\boldsymbol{\phi}^\star$.

The proof is given in Appendix A.

Due to Lemma 2, (17b) and (17c) jointly enforce the optimal solution of (17) to satisfy $\boldsymbol{\omega}^\star = \mathbb{0}_n$. The variable substitution from $\boldsymbol{\theta}$ to $\boldsymbol{\phi}$ is necessary for embedding dynamics (1) in primal-dual algorithm while preserving constraints (2)(3)(4).

The linear relationship $P_{ij} = B_{ij}(\theta_i - \theta_j)$ makes the combination of (17d) and (17e) equivalent to line thermal limits (3) with $\overline{\boldsymbol{\theta}} := \boldsymbol{B}^{-1}\overline{\boldsymbol{P}}$ and $\underline{\boldsymbol{\theta}} := \boldsymbol{B}^{-1}\underline{\boldsymbol{P}}$.

Now, the Lagrangian function associated with problem (17) is given by

$$\begin{aligned} L = {} & \frac{1}{2}\boldsymbol{\omega}^T\boldsymbol{A}\boldsymbol{\omega} + \frac{1}{2}\boldsymbol{u}^T\boldsymbol{\Xi}\boldsymbol{L}_Q\boldsymbol{\Xi}\boldsymbol{u} \\ & + \boldsymbol{\nu}^T\left(\boldsymbol{u} - \boldsymbol{p} - \boldsymbol{A}\boldsymbol{\omega} - \boldsymbol{C}\boldsymbol{B}\boldsymbol{C}^T\boldsymbol{\theta}\right) \\ & + \boldsymbol{\lambda}^T\left(\boldsymbol{u} - \boldsymbol{p} - \boldsymbol{C}\boldsymbol{B}\boldsymbol{C}^T\boldsymbol{\phi}\right) \\ & + (\boldsymbol{\eta}^+)^T(\boldsymbol{C}^T\boldsymbol{\phi} - \overline{\boldsymbol{\theta}}) + (\boldsymbol{\eta}^-)^T(\underline{\boldsymbol{\theta}} - \boldsymbol{C}^T\boldsymbol{\phi})\,. \end{aligned} \tag{18}$$

The Lagrangian function above is actually a saddle function that is convex to primal variables $\boldsymbol{x} := (\boldsymbol{\theta}, \boldsymbol{\omega}, \boldsymbol{u}, \boldsymbol{\phi})$ and concave to dual variables $\boldsymbol{\rho} := (\boldsymbol{\nu}, \boldsymbol{\lambda}, \boldsymbol{\eta}^+, \boldsymbol{\eta}^-)$, which is essential for the proof of asymptotic stability.

Remark 1: Power rating constraint (17f) is not included in (18) since it will be enforced by inheriting the form of (16c) in the following controller design.

For the following controller design and stability analysis, we consider three changes of variables $\tilde{\boldsymbol{\theta}} := \boldsymbol{C}^T\boldsymbol{\theta}$, $\boldsymbol{u} = \boldsymbol{K}\boldsymbol{\xi}$, and $\tilde{\boldsymbol{\phi}} := \boldsymbol{C}^T\boldsymbol{\phi}$. Thus, the subsequent analysis will be conducted with respect to $\tilde{\boldsymbol{x}} := (\tilde{\boldsymbol{\theta}}, \boldsymbol{\omega}, \boldsymbol{u}, \tilde{\boldsymbol{\phi}})$ instead of $\boldsymbol{x}$. These three linear bijections do not affect the dynamics of the variables or the stability of the system.

With the same approach and conclusion that $\boldsymbol{\omega}(t) \equiv \boldsymbol{\nu}(t)$ in Section IV-A, we design the following enhanced DAI controller based on the gradient flow of the Lagrangian function (18):

$$\dot{\boldsymbol{u}} = \left[\boldsymbol{u} - \boldsymbol{\omega} - \boldsymbol{\lambda} - \boldsymbol{\Xi}\boldsymbol{L}_Q\boldsymbol{\Xi}\boldsymbol{u}\right]_{\underline{\boldsymbol{u}}}^{\overline{\boldsymbol{u}}} - \boldsymbol{u} \tag{19a}$$

$$\dot{\tilde{\boldsymbol{\phi}}} = \boldsymbol{\Gamma}^{\tilde{\phi}}(\boldsymbol{B}\boldsymbol{C}^T\boldsymbol{\lambda} - \boldsymbol{\eta}^+ + \boldsymbol{\eta}^-) \tag{19b}$$

$$\dot{\boldsymbol{\lambda}} = \boldsymbol{\Gamma}^{\lambda}(\boldsymbol{u} - \boldsymbol{p} - \boldsymbol{C}\boldsymbol{B}\tilde{\boldsymbol{\phi}}) \tag{19c}$$

$$\dot{\boldsymbol{\eta}}^+ = \boldsymbol{\Gamma}^{\eta}\left[\tilde{\boldsymbol{\phi}} - \overline{\boldsymbol{\theta}}\right]_{\boldsymbol{\eta}^+}^+ \tag{19d}$$

$$\dot{\boldsymbol{\eta}}^- = \boldsymbol{\Gamma}^{\eta}\left[\underline{\boldsymbol{\theta}} - \tilde{\boldsymbol{\phi}}\right]_{\boldsymbol{\eta}^-}^+ \tag{19e}$$

where $\boldsymbol{\Gamma}^{\lambda} := \text{diag}(\gamma_i^{\lambda}, i \in \mathcal{V})$, $\boldsymbol{\Gamma}^{\tilde{\phi}} := \text{diag}(\gamma_{ij}^{\tilde{\phi}},\ (i,j) \in \mathcal{E})$, and $\boldsymbol{\Gamma}^{\eta} := \text{diag}(\gamma_{ij}^{\eta},\ (i,j) \in \mathcal{E})$ are all positive definite constant matrices. The element-wise operator $[\boldsymbol{y}]_{\boldsymbol{\eta}}^+$ is defined as

$$[y_i]_{\eta_i}^+ := \begin{cases} y_i & \text{if} \quad \eta_i > 0 \text{ or } \quad y_i > 0\,, \\ 0 & \text{otherwise.} \end{cases} \tag{20}$$

This projection is active ($[y_i]_{\eta_i}^+ = 0$) only if $y_i \le 0$ and $\eta_i \le 0$, and thus, $[y_i]_{\eta_i}^+(\eta_i - \eta_i^*) = 0 \le y_i(\eta_i - \eta_i^*)$.

We now illustrate the relationship between the primal-dual optimal solution of optimization problem (17) and the equilibrium of closed-loop system (1), (19) by the following theorem.

Theorem 1: Suppose (17) is feasible. A point $\tilde{\boldsymbol{z}}^* := (\tilde{\boldsymbol{\theta}}^*, \boldsymbol{\omega}^*, \boldsymbol{u}^*, \tilde{\boldsymbol{\phi}}^*, \boldsymbol{\lambda}^*, \boldsymbol{\eta}^{+*}, \boldsymbol{\eta}^{-*})$ satisfying $\underline{u}_i \le {u_i}^* \le \overline{u}_i$ and $\underline{P}_{ij} \le B_{ij}(\theta_i^* - \theta_j^*) \le \overline{P}_{ij}$ is an equilibrium of closed-loop system (1), (19) if and only if $\tilde{\boldsymbol{z}}^*$ is the primal-dual optimal solution of (17), with $\boldsymbol{\omega}^* = \mathbb{0}_n$.

The proof is given in Appendix B.

To simplify the notation, we define a new vector function $\boldsymbol{G}(\tilde{\boldsymbol{z}})$ on system state $\tilde{\boldsymbol{z}} := (\tilde{\boldsymbol{\theta}}, \boldsymbol{\omega}, \boldsymbol{u}, \tilde{\boldsymbol{\phi}}, \boldsymbol{\lambda}, \boldsymbol{\eta}^+, \boldsymbol{\eta}^-)$

$$\boldsymbol{G}(\tilde{\boldsymbol{z}}) = \begin{bmatrix} -\boldsymbol{B}^{\frac{1}{2}}\boldsymbol{C}^T\boldsymbol{\omega} \\ -\boldsymbol{M}^{-\frac{1}{2}}\left(\boldsymbol{u} - \boldsymbol{p} - \boldsymbol{A}\boldsymbol{\omega} - \boldsymbol{C}\boldsymbol{B}\tilde{\boldsymbol{\theta}}\right) \\ \boldsymbol{\omega} + \boldsymbol{\lambda} + \boldsymbol{\Xi}\boldsymbol{L}_Q\boldsymbol{\Xi}\boldsymbol{u} \\ (\boldsymbol{\Gamma}^{\tilde{\phi}})^{\frac{1}{2}}(-\boldsymbol{B}\boldsymbol{C}^T\boldsymbol{\lambda} + \boldsymbol{\eta}^+ - \boldsymbol{\eta}^-) \\ -(\boldsymbol{\Gamma}^{\lambda})^{\frac{1}{2}}(\boldsymbol{u} - \boldsymbol{p} - \boldsymbol{C}\boldsymbol{B}\tilde{\boldsymbol{\phi}}) \\ -(\boldsymbol{\Gamma}^{\eta})^{\frac{1}{2}}\left[\tilde{\boldsymbol{\phi}} - \overline{\boldsymbol{\theta}}\right]_{\boldsymbol{\eta}^+}^+ \\ -(\boldsymbol{\Gamma}^{\eta})^{\frac{1}{2}}\left[\underline{\boldsymbol{\theta}} - \tilde{\boldsymbol{\phi}}\right]_{\boldsymbol{\eta}^-}^+ \end{bmatrix} \tag{21}$$

Based on $\boldsymbol{G}(\tilde{\boldsymbol{z}})$, we then defined another vector function involving projection

$$\boldsymbol{H}(\tilde{\boldsymbol{z}}) = \begin{bmatrix} \boldsymbol{B}^{\frac{1}{2}}\boldsymbol{C}^T\boldsymbol{\omega} \\ \boldsymbol{M}^{-\frac{1}{2}}(\boldsymbol{u}-\boldsymbol{p}-\boldsymbol{A}\boldsymbol{\omega}-\boldsymbol{C}\boldsymbol{B}\tilde{\boldsymbol{\theta}}) \\ \left[\boldsymbol{u}-(\boldsymbol{\omega}+\boldsymbol{\lambda}+\boldsymbol{\Xi}\boldsymbol{L}_Q\boldsymbol{\Xi}\boldsymbol{u})\right]_{\underline{\boldsymbol{u}}}^{\overline{\boldsymbol{u}}}-\boldsymbol{u} \\ (\boldsymbol{\Gamma}^{\tilde{\phi}})^{\frac{1}{2}}(\boldsymbol{B}\boldsymbol{C}^T\boldsymbol{\lambda}-\boldsymbol{\eta}^+ +\boldsymbol{\eta}^-) \\ (\boldsymbol{\Gamma}^{\lambda})^{\frac{1}{2}}(\boldsymbol{u}-\boldsymbol{p}-\boldsymbol{C}\boldsymbol{B}\tilde{\boldsymbol{\phi}}) \\ (\boldsymbol{\Gamma}^{\eta})^{\frac{1}{2}}\left[\tilde{\boldsymbol{\phi}}-\overline{\boldsymbol{\theta}}\right]_{\boldsymbol{\eta}^+}^{+} \\ (\boldsymbol{\Gamma}^{\eta})^{\frac{1}{2}}\left[\underline{\boldsymbol{\theta}}-\tilde{\boldsymbol{\phi}}\right]_{\boldsymbol{\eta}^-}^{+} \end{bmatrix} \tag{22}$$

and $\boldsymbol{H}(\tilde{\boldsymbol{z}}) = \text{Proj}_S(\tilde{\boldsymbol{z}}-\boldsymbol{G}(\tilde{\boldsymbol{z}}))-\tilde{\boldsymbol{z}}$ where $S \subseteq \mathbb{R}^{3|\mathcal{V}|+4|\mathcal{E}|}$ is the feasible region with (4). Thus, the closed-loop system (1), (19) can be rewritten as

$$\dot{\tilde{\boldsymbol{z}}}(t) = \boldsymbol{\Gamma}\boldsymbol{H}(\tilde{\boldsymbol{z}}(t)) \tag{23}$$

where

$$\boldsymbol{\Gamma} = \text{diag}(\boldsymbol{B}^{-\frac{1}{2}}, \boldsymbol{M}^{-\frac{1}{2}}, \boldsymbol{I}, (\boldsymbol{\Gamma}^{\tilde{\phi}})^{\frac{1}{2}}, (\boldsymbol{\Gamma}^{\lambda})^{\frac{1}{2}}, (\boldsymbol{\Gamma}^{\eta})^{\frac{1}{2}}, (\boldsymbol{\Gamma}^{\eta})^{\frac{1}{2}})$$

is a positive definite diagonal matrix.

C. Stability Analysis

For system (23), $\tilde{\boldsymbol{z}}^*$ is an equilibrium point if and only if $\boldsymbol{H}(\tilde{\boldsymbol{z}}^*) = \mathbb{0}_{3|\mathcal{V}|+4|\mathcal{E}|}$, i.e., a fixed point of projection. Then we have the following theorem.

Theorem 2: Suppose (17) is feasible. If the closed-loop system (23) starts from initial state with $\underline{\boldsymbol{u}} \le \boldsymbol{u}(0) \le \overline{\boldsymbol{u}}$, it will asymptotically converge to $\tilde{\boldsymbol{z}}^*$, which is one specific equilibrium point. $\boldsymbol{u}(t)$ will be bounded in $\underline{\boldsymbol{u}} \le \boldsymbol{u}(t) \le \overline{\boldsymbol{u}}$.

The proof is given in Appendix C.

Since the projection in (19d) and (19e) introduces non-smoothness, it is challenging to directly construct a differentiable Lyapunov function to prove asymptotic stability of the system. By following [15], we first consider two sets concerning constraints (17d) and (17e).

$$\sigma^+ := \left\{(i,j) \in \mathcal{E} | \eta_{ij}^+ = 0, \tilde{\phi}_{ij} - \overline{\theta}_{ij} < 0\right\} \tag{24a}$$

$$\sigma^- := \left\{(i,j) \in \mathcal{E} | \eta_{ij}^- = 0, \underline{\theta}_{ij} - \tilde{\phi}_{ij} < 0\right\} \tag{24b}$$

The non-smoothness of a function involving $\boldsymbol{\eta}^+$ and $\boldsymbol{\eta}^-$, such as $\boldsymbol{G}(\tilde{\boldsymbol{z}})$ and $\boldsymbol{H}(\tilde{\boldsymbol{z}})$, can be attributed to the fact that these two sets are not fixed. To proceed, we first assume that σ^+ and σ^- are fixed, so that $\boldsymbol{G}(\tilde{\boldsymbol{z}})$ becomes continuously differentiable.

As a step toward designing an appropriate Lyapunov function to establish the asymptotic stability of the system (23), we begin by considering the following function under the assumption that σ^+ and σ^- are fixed, as follows [11].

$$\hat{V}(\tilde{\boldsymbol{z}}) = -(\boldsymbol{H}(\tilde{\boldsymbol{z}}))^T\boldsymbol{G}(\tilde{\boldsymbol{z}}) - \frac{1}{2}\|\boldsymbol{H}(\tilde{\boldsymbol{z}})\|_2^2 \tag{25a}$$

$$+ \frac{1}{2}\gamma\left(\tilde{\boldsymbol{z}}-\tilde{\boldsymbol{z}}^*\right)^T\boldsymbol{\Gamma}^{-2}\left(\tilde{\boldsymbol{z}}-\tilde{\boldsymbol{z}}^*\right), \tag{25b}$$

where γ is a sufficiently small constant such that $\boldsymbol{\Gamma}-\gamma\boldsymbol{\Gamma}^{-1}$ is strictly positive definite, which is a neccessary condition for proving the non-increasing of $\hat{V}(\tilde{\boldsymbol{z}})$.

Maintaining the assumption that σ^+ and σ^- are fixed, $\hat{V}(\tilde{\boldsymbol{z}})$ is a continuously differentiable function. Then we claim that $\hat{V}(\tilde{\boldsymbol{z}}) \ge 0$, with equality if and only if the system is at the equilibrium point $\tilde{\boldsymbol{z}}^*$ [16], and $\dot{\hat{V}}(\tilde{\boldsymbol{z}}) \le 0$.

Nonfixed σ^+ and σ^- lead to the discontinuity of the function $\hat{V}(\tilde{\boldsymbol{z}})$ at certain points. To address this issue, we modify the values of $\hat{V}(\tilde{\boldsymbol{z}})$ at these particular points based on the idea of the Clarke generalized derivative [17, p. 27], thereby constructing the candidate Lyapunov function below.

$$V(\tilde{\boldsymbol{z}}) := \begin{cases} \hat{V}(\tilde{\boldsymbol{z}}), & \hat{V}(\tilde{\boldsymbol{z}}) \text{ is continuous at } \tilde{\boldsymbol{z}}, \\ \lim_{\tilde{\boldsymbol{z}}' \to \tilde{\boldsymbol{z}}} \sup \hat{V}(\tilde{\boldsymbol{z}}'), & \text{otherwise.} \end{cases} \tag{26}$$

We will also prove that non-increasing function $V(\tilde{\boldsymbol{z}}) \ge 0$ in feasible region and equality holds only at $\tilde{\boldsymbol{z}}^*$ with $\boldsymbol{H}(\tilde{\boldsymbol{z}}^*) = \mathbb{0}_{3|\mathcal{V}|+4|\mathcal{E}|}$.

V. Numerical Results

In this section, we present the simulation results conducted on the IEEE 39-bus system (New England) [18], which contains 39 buses and 46 lines. Originally, each bus indexed by $i \in \{30, \cdots, 39\}$ had a single generator. To adapt to the power system in this study, we added an additional generator to buses indexed by $i \in \{1, \cdots, 29\}$, ensuring that each node has exactly one generator. The inertia parameters of the generators at bus $i \in \{30, \cdots, 39\}$ is obtained from the Power System Toolbox [19], while the generators added at bus $i \in \{1, \cdots, 29\}$ are assigned a uniform inertia value, which is approximately the median of the inertia values of the generators at bus $i \in \{30, \cdots, 39\}$. The droop coefficient is $\alpha_i = 150$ p.u., $\forall i \in \mathcal{V}$. We apply a step change of $p_i = 2$ p.u. in uncontrollable load at bus $i \in \{14, 22, 28\}$, respectively.

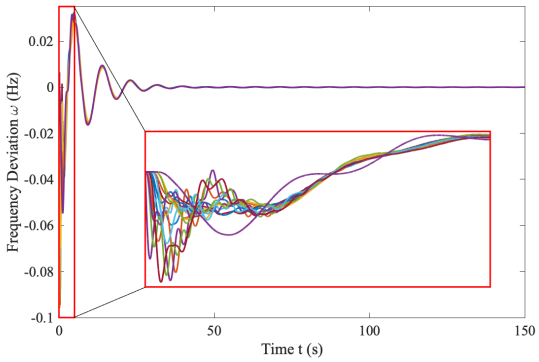

Fig. 1: Frequency Deviation

The first result in Figure 1 demonstrates that the designed controller successfully drives the system frequency back to its pre-disturbance value (50 Hz or 60 Hz), indicating the achievement of secondary frequency control. During the approximately 30 seconds required for frequency stabilization, the system exhibits only a minor overshoot of about 0.03 Hz. The controller responds rapidly, limiting the maximum frequency deviation following the disturbance to less than

0.1 Hz. The purple line in the figure represents the frequency trajectory at bus 39. According to the parameters provided by the Power System Toolbox, the generator at bus 39 possesses significantly larger inertia compared to those at other buses. As a result, the frequency at bus 39 changes more gradually, exhibiting stronger disturbance rejection and better stability.

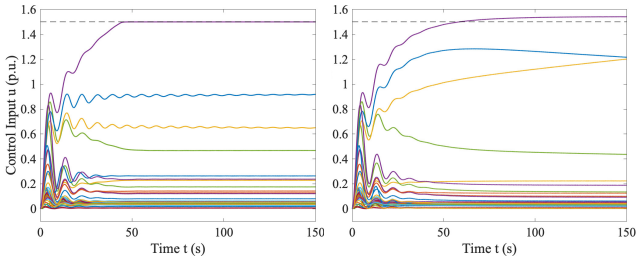

Fig. 2: Generated power at each bus with (left) / without (right) generator capacity constraints.

The generation capacity of each generator is set to a maximum of 1.5 p.u.. Figure 2 shows the generated power at each bus with and without the enforcement of power rating constraints to the generators. The comparison reveals that the constrained controller successfully enforces power rating constraints even during the transient, without compromising frequency restoration or system stability.

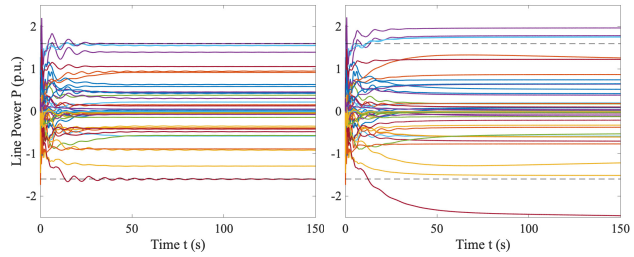

Fig. 3: Line power with (left) / without (right) line thermal limits.

In Figure 3, we compared the convergence of line power flows with and without the enforcement of line thermal limits. Unlike generator capacity, the line thermal limits $[-1.6, 1.6]$ in p.u. are required to be satisfied only at steady state. The results demonstrate that the proposed controller successfully enforces these constraints after the system reaches equilibrium, without compromising frequency restoration or overall system stability. In contrast, the traditional DAI controller fails to respect the line limits, resulting in power flows that exceed thermal capacities on certain lines.

VI. Conclusion

In this paper, we proposed an enhanced distributed averaging-based integral (DAI) controller that ensures the closed-loop system remains within operational constraints while stabilizing the system and restoring frequency to its nominal value. From the perspective of the primal-dual algorithm, the control problem is reformulated as an equivalent constrained optimization problem, allowing operational constraints to be systematically integrated through the optimization process. This perspective motivates the reinterpretation of the control problem with constraints through primal-dual dynamics, enabling the characterization of system equilibrium points and convergence trajectories via the saddle points of the associated Lagrangian. Furthermore, the inherent monotonicity of the saddle function's gradient forms the basis for analyzing key structural properties of the controller—such as monotonicity and convexity—which are instrumental in extending the framework to more general control architectures.

References

[1] C. Zhao, U. Topcu, N. Li, and S. Low, "Design and stability of load-side primary frequency control in power systems," *IEEE Transactions on Automatic Control*, vol. 59, no. 5, pp. 1177–1189, May 2014.

[2] F. Dörfler and S. Grammatico, "Gather-and-broadcast frequency control in power systems," *Automatica*, vol. 79, pp. 296–305, May 2017.

[3] J. Schiffer, F. Dörfler, and E. Fridman, "Robustness of distributed averaging control in power systems: Time delays & dynamic communication topology," *Automatica*, vol. 80, pp. 261–271, June 2017.

[4] J. Schiffer and F. Dörfler, "On stability of a distributed averaging PI frequency and active power controlled differential-algebraic power system model," in *Proc. of European Control Conference*, June 2016, pp. 1487–1492.

[5] F. Dörfler, J. W. Simpson-Porco, and F. Bullo, "Breaking the hierarchy: Distributed control and economic optimality in microgrids," *IEEE Transactions on Control of Network Systems*, vol. 3, no. 3, pp. 241–253, 2015.

[6] E. Weitenberg, C. De Persis, and N. Monshizadeh, "Exponential convergence under distributed averaging integral frequency control," *Automatica*, vol. 98, pp. 103–113, Dec. 2018.

[7] Y. Jiang, W. Cui, B. Zhang, and J. Cortés, "Stable reinforcement learning for optimal frequency control: A distributed averaging-based integral approach," *IEEE Open Journal of Control Systems*, vol. 1, pp. 194–209, Aug. 2022.

[8] N. Li, C. Zhao, and L. Chen, "Connecting automatic generation control and economic dispatch from an optimization view," *IEEE Transactions on Control of Network Systems*, vol. 3, no. 3, pp. 254–264, Sept. 2016.

[9] E. Mallada, C. Zhao, and S. Low, "Optimal load-side control for frequency regulation in smart grids," *IEEE Transactions on Automatic Control*, vol. 62, no. 12, pp. 6294–6309, Dec. 2017.

[10] P. You, Y. Jiang, E. Yeung, D. F. Gayme, and E. Mallada, "On the stability, economic efficiency and incentive compatibility of electricity market dynamics," *arxiv preprint: 2112.05811*, 2021.

[11] Z. Wang, F. Liu, S. H. Low, C. Zhao, and S. Mei, "Distributed frequency control with operational constraints, part II: Network power balance," *IEEE Transactions on Smart Grid*, vol. 10, no. 1, pp. 53–64, Jan. 2019.

[12] P. You, J. Z. Pang, and E. Yeung, "Stabilization of power networks via market dynamics," in *Proceedings of the Ninth International Conference on Future Energy Systems*, 2018, pp. 139–145.

[13] C. Zhao, E. Mallada, and F. Dörfler, "Distributed frequency control for stability and economic dispatch in power networks," in *Proc. of American Control Conference*, July 2015, pp. 2359–2364.

[14] D. Cai, E. Mallada, and A. Wierman, "Distributed optimization decomposition for joint economic dispatch and frequency regulation," *IEEE Transactions on Power Systems*, vol. 32, no. 6, pp. 4370–4385, 2017.

[15] D. Feijer and F. Paganini, "Stability of primal–dual gradient dynamics and applications to network optimization," *Automatica*, vol. 46, no. 12, pp. 1974–1981, 2010.

[16] M. Fukushima, "Equivalent differentiable optimization problems and descent methods for asymmetric variational inequality problems," *Mathematical programming*, vol. 53, pp. 99–110, 1992.

[17] F. H. Clarke, *Optimization and nonsmooth analysis*. SIAM, 1990.

[18] T. Athay, R. Podmore, and S. Virmani, "A practical method for the direct analysis of transient stability," *IEEE Transactions on Power Apparatus and Systems*, no. 2, pp. 573–584, Mar. 1979.

[19] J. H. Chow and K. W. Cheung, "A toolbox for power system dynamics and control engineering education and research," *IEEE transactions on Power Systems*, vol. 7, no. 4, pp. 1559–1564, Nov. 1992.

APPENDIX

A. Proof of Lemma 2

Before proving $\boldsymbol{C}^T\boldsymbol{\theta}^\star = \boldsymbol{C}^T\boldsymbol{\phi}^\star$, we first prove that $\boldsymbol{\omega}^\star = \mathbb{0}_n$.

By premultiplying (17b) and (17c) with $\mathbb{1}_n$, we have

$$\mathbb{1}_n^T(\boldsymbol{u}^\star - \boldsymbol{p}^\star - \boldsymbol{A}\boldsymbol{\omega}^\star) = \mathbb{1}_n^T\boldsymbol{C}\boldsymbol{B}\boldsymbol{C}^T\boldsymbol{\theta}^\star = 0$$

$$\mathbb{1}_n^T(\boldsymbol{u}^\star - \boldsymbol{p}^\star) = \mathbb{1}_n^T\boldsymbol{C}\boldsymbol{B}\boldsymbol{C}^T\boldsymbol{\phi}^\star = 0$$

Thus, $\boldsymbol{\omega}^\star = \mathbb{0}_n$.

Now we give the proof of *Lemma* 2.

Since the graph $(\mathcal{V}, \mathcal{E})$ is connected, we have $\text{rank}(\boldsymbol{C}\boldsymbol{B}\boldsymbol{C}^T) = n-1$. Thus, the null space has dimension 1, which is spanned by vector $\mathbb{1}_n$ because of $\mathbb{1}_n^T\boldsymbol{C} = \mathbb{0}_{|\mathcal{E}|}$.

According to $\boldsymbol{\omega}^\star = \mathbb{0}_n$, we have $\boldsymbol{C}\boldsymbol{B}\boldsymbol{C}^T(\boldsymbol{\phi}^\star - \boldsymbol{\theta}^\star) = \mathbb{0}_n$. Hence we have $\boldsymbol{\phi}^\star - \boldsymbol{\theta}^\star = (\phi_0 - \theta_0)\mathbb{1}_n$ where $\phi_0 - \theta_0$ is a constant that can be referred to reference virtual angle and reference phase angle. Then we have $\boldsymbol{C}^T\boldsymbol{\theta}^\star = \boldsymbol{C}^T\boldsymbol{\phi}^\star$.

B. Proof of Theorem 1

We first characterize the primal-dual optimality conditions of optimization problem (17). The objective function and all constraints in (17) are convex, and the operational constraints are bounded. Moreover, a strictly feasible solution exists that satisfies all the constraints. Therefore, Slater condition holds for this problem.

According to the strong duality theorem, $\boldsymbol{z}^* = (\boldsymbol{\theta}^*, \boldsymbol{\omega}^*, \boldsymbol{u}^*, \boldsymbol{\phi}^*, \boldsymbol{\nu}^*, \boldsymbol{\lambda}^*, \boldsymbol{\eta}^{+^*}, \boldsymbol{\eta}^{-^*})$ is primal-dual optimal of (17) if and only if:

1) Primal feasible: $(\boldsymbol{\theta}^*, \boldsymbol{\omega}^*, \boldsymbol{u}^*, \boldsymbol{\phi}^*)$ satisfies (17b)-(17f).
2) Dual feasible: $\boldsymbol{\eta}^{+^*} \geq 0$, $\boldsymbol{\eta}^{-^*} \geq 0$.
3) Stationarity: At $\boldsymbol{z}^*$, the gradient of the Lagrangian function (18) is equal to zero.
4) Complementary slackness:

$$\eta_{ij}^{+^*}((\phi_i^* - \phi_j^*) - \overline{\theta}_{ij}) = 0$$

$$\eta_{ij}^{-^*}(\underline{\theta}_{ij} - (\phi_i^* - \phi_j^*)) = 0$$

Thus,

$$\nabla F(\boldsymbol{u}^*) + \boldsymbol{\omega}^* + \boldsymbol{\lambda}^* = 0$$

$$\boldsymbol{\omega}^* = \boldsymbol{\nu}^* = \mathbb{0}_n$$

$$\boldsymbol{C}^T\boldsymbol{\nu} = \mathbb{0}_{|\mathcal{E}|}$$

and due to the cost function is strictly convex to $\boldsymbol{\omega}$, it is easy to show that $\boldsymbol{\omega}^* = \boldsymbol{\nu}^*$ is unique. As we have proven in *Lemma* 2, $\boldsymbol{\omega}^* = \mathbb{0}_n$.

Based on the definition of primal-dual optimal above, we now proof Theorem 1.

If $\tilde{\boldsymbol{z}}^*$ is an equilibrium point of system (1) and (19), and satisfies the operational constraints (4) (3), then $\dot{\tilde{\boldsymbol{z}}}^* = 0$ and $\underline{\boldsymbol{\theta}} \leq \tilde{\boldsymbol{\phi}}^* \leq \overline{\boldsymbol{\theta}}$. Therefore, $\tilde{\boldsymbol{z}}^*$ satisfies (1) and (19), i.e., primal feasibility and stationarity. Furthermore, due to (19d) and (19e), we have $\boldsymbol{\eta}^{+^*}, \boldsymbol{\eta}^{-^*} \geq 0$, which ensures dual feasibility and complementary slackness. Then equilibrium $\tilde{\boldsymbol{z}}^*$ is the primal-dual optimal of (17).

Conversely, if a point $\tilde{\boldsymbol{z}}^*$ is a primal dual optimal of (17), then stationarity as well as operational constraints are satisfied, which implies $\dot{\tilde{\boldsymbol{z}}}^* = 0$, i.e., the equilibrium of closed-loop system.

C. Proof of Theorem 2

We first assume that $\sigma+$ and σ^- are both fixed sets. Under this assumption, we prove that $\hat{V}(\tilde{\boldsymbol{z}}) \geq 0$.

Let $\hat{V}_1(\tilde{\boldsymbol{z}}) = -(\boldsymbol{H}(\tilde{\boldsymbol{z}}))^T\boldsymbol{G}(\tilde{\boldsymbol{z}}) - \frac{1}{2}\|\boldsymbol{H}(\tilde{\boldsymbol{z}})\|_2^2$, $\hat{V}_2(\tilde{\boldsymbol{z}}) = \frac{1}{2}\gamma\left(\tilde{\boldsymbol{z}} - \tilde{\boldsymbol{z}}^*\right)^T\boldsymbol{\Gamma}^{-2}\left(\tilde{\boldsymbol{z}} - \tilde{\boldsymbol{z}}^*\right)$. According to [16, Th. 3.1], $\hat{V}_1(\tilde{\boldsymbol{z}}) \geq 0$ in feasible region S and the equality holds only at an equilibrium point $\tilde{\boldsymbol{z}}^*$ with $\boldsymbol{H}(\tilde{\boldsymbol{z}}^*) = \mathbb{0}_{3|\mathcal{V}|+4|\mathcal{E}|}$. The second term $\hat{V}_2(\tilde{\boldsymbol{z}})$ is quadratic with $\gamma > 0$ and $\boldsymbol{\Gamma} \succ 0$. Then we have $\hat{V}(\tilde{\boldsymbol{z}}) \geq 0$ and equality holds only at an equilibrium point.

Then we prove that $\dot{\hat{V}}(\tilde{\boldsymbol{z}}) \leq 0$ with fixed σ^+ and σ^-.

For all $(i,j) \notin \sigma^+$,$(i,j) \notin \sigma^-$

$$\begin{aligned}
\dot{\hat{V}}(\tilde{\boldsymbol{z}}) =& \nabla_{\tilde{\boldsymbol{z}}}^T\hat{V}(\tilde{\boldsymbol{z}})\dot{\tilde{\boldsymbol{z}}} = \nabla_{\tilde{\boldsymbol{z}}}^T\hat{V}(\tilde{\boldsymbol{z}}) \cdot \boldsymbol{\Gamma}\boldsymbol{H}(\tilde{\boldsymbol{z}}) && \text{(27a)}\\
\leq& \gamma\left(\boldsymbol{H}(\tilde{\boldsymbol{z}}) + \tilde{\boldsymbol{z}} - \tilde{\boldsymbol{z}}^*\right)^T \cdot \boldsymbol{\Gamma}^{-1}(\boldsymbol{H}(\tilde{\boldsymbol{z}}) + \boldsymbol{G}(\tilde{\boldsymbol{z}})) && \text{(27b)}\\
&+ \left(\boldsymbol{H}(\tilde{\boldsymbol{z}}) + \boldsymbol{G}(\tilde{\boldsymbol{z}})\right)^T\left(\boldsymbol{\Gamma} - \gamma\boldsymbol{\Gamma}^{-1}\right)\boldsymbol{H}(\tilde{\boldsymbol{z}}) && \text{(27c)}\\
&- \left(\boldsymbol{H}(\tilde{\boldsymbol{z}})\right)^T\nabla_{\tilde{\boldsymbol{z}}}\boldsymbol{G}(\tilde{\boldsymbol{z}}) \cdot \boldsymbol{\Gamma}\boldsymbol{H}(\tilde{\boldsymbol{z}}) && \text{(27d)}\\
&- \gamma\left(\tilde{\boldsymbol{z}} - \tilde{\boldsymbol{z}}^*\right)^T \cdot \boldsymbol{\Gamma}^{-1}\boldsymbol{G}(\tilde{\boldsymbol{z}}) && \text{(27e)}
\end{aligned}$$

According to projection theorem,

$$\text{Proj}_{S,\boldsymbol{\Gamma}}(\tilde{\boldsymbol{z}}) := \arg\min_{\boldsymbol{y}\in\boldsymbol{S}}(\boldsymbol{y} - \tilde{\boldsymbol{z}})^T\boldsymbol{\Gamma}(\boldsymbol{y} - \tilde{\boldsymbol{z}})$$

and $\tilde{\boldsymbol{z}}^\dagger = \text{Proj}_{S,\boldsymbol{\Gamma}}(\tilde{\boldsymbol{z}})$ if and only if $(\tilde{\boldsymbol{z}}^\dagger - \tilde{\boldsymbol{z}})^T\boldsymbol{\Gamma}(\boldsymbol{y} - \tilde{\boldsymbol{z}}^\dagger) \geq 0$ with $\boldsymbol{y} \in S$.

For (27b) and (27c), $\tilde{\boldsymbol{z}} \in S$ along the trajectory and $\tilde{\boldsymbol{z}}^* \in S$. Since $\boldsymbol{H}(\tilde{\boldsymbol{z}}) + \tilde{\boldsymbol{z}} = \text{Proj}_S(\tilde{\boldsymbol{z}} - \boldsymbol{G}(\tilde{\boldsymbol{z}}))$ and $\boldsymbol{\Gamma} - \gamma\boldsymbol{\Gamma}^{-1} \succ 0$, the right side of (27b) and (27c) are non-positive.

For (27d), we have $\nabla_{\tilde{\boldsymbol{z}}}G(\tilde{\boldsymbol{z}})$ shown in (28), where $\boldsymbol{\Gamma} \succ 0$ and $\boldsymbol{D} \succeq 0$. Hence the right side of (27d) is non-positive.

For (27e), by substituting $\boldsymbol{\nu}$ with $\boldsymbol{\omega}$, Lagrangian function $L(\tilde{\boldsymbol{z}})$ is convex with repect to $\tilde{\boldsymbol{z}}_1 := (\tilde{\boldsymbol{\theta}}, \boldsymbol{u}, \tilde{\boldsymbol{\phi}})$ while concave to $\tilde{\boldsymbol{z}}_2 := (\boldsymbol{\omega}, \boldsymbol{\lambda}, \boldsymbol{\eta}^+, \boldsymbol{\eta}^-)$. Specially, we have

$$(\boldsymbol{\eta}^+ - \boldsymbol{\eta}^{+^*})^T[\tilde{\boldsymbol{\phi}} - \overline{\boldsymbol{\theta}}]_{\boldsymbol{\eta}^+}^+ \leq (\boldsymbol{\eta}^+ - \boldsymbol{\eta}^{+^*})^T(\tilde{\boldsymbol{\phi}} - \overline{\boldsymbol{\theta}})$$

$$(\boldsymbol{\eta}^- - \boldsymbol{\eta}^{-^*})^T[\underline{\boldsymbol{\theta}} - \tilde{\boldsymbol{\phi}}]_{\boldsymbol{\eta}^-}^+ \leq (\boldsymbol{\eta}^- - \boldsymbol{\eta}^{-^*})^T(\underline{\boldsymbol{\theta}} - \tilde{\boldsymbol{\phi}})$$

Hence we have

$$\begin{aligned}
&-\gamma\left(\tilde{\boldsymbol{z}} - \tilde{\boldsymbol{z}}^*\right)^T \cdot \boldsymbol{\Gamma}^{-1}\boldsymbol{G}(\tilde{\boldsymbol{z}})\\
=& -\gamma(\tilde{\boldsymbol{z}}_1 - \tilde{\boldsymbol{z}}_1^*)^T\nabla_{\tilde{\boldsymbol{z}}_1}L(\tilde{\boldsymbol{z}}_1, \tilde{\boldsymbol{z}}_2)\\
&+ \gamma(\tilde{\boldsymbol{z}}_2 - \tilde{\boldsymbol{z}}_2^*)^T\nabla_{\tilde{\boldsymbol{z}}_2}L(\tilde{\boldsymbol{z}}_1, \tilde{\boldsymbol{z}}_2)\\
&\leq \gamma\Big(L(\tilde{\boldsymbol{z}}_1^*, \tilde{\boldsymbol{z}}_2) - L(\tilde{\boldsymbol{z}}_1, \tilde{\boldsymbol{z}}_2) + L(\tilde{\boldsymbol{z}}_1, \tilde{\boldsymbol{z}}_2) - L(\tilde{\boldsymbol{z}}_1, \tilde{\boldsymbol{z}}_2^*)\Big)\\
&\leq 0
\end{aligned}$$

Consequently, we have $\dot{\hat{V}}(\tilde{\boldsymbol{z}}) \leq 0$ with fixed σ^+ and σ^-.

Now we consider the case that σ^+ is changed.

1) σ^+ is reduced. This only occurs when $\tilde{\boldsymbol{\phi}} - \overline{\boldsymbol{\theta}}$ switches from a negative to a positive value. In this case, $\boldsymbol{\eta}^+$ turns to positive from zero and no discontinuity occurs.

$$
\begin{aligned}
\nabla_{\tilde{\boldsymbol{z}}}\boldsymbol{G}(\tilde{\boldsymbol{z}}) &= \begin{bmatrix}
0 & -\boldsymbol{B}^{\frac{1}{2}}\boldsymbol{C}^T & 0 & 0 & 0 & 0 & 0 \\
\boldsymbol{M}^{-\frac{1}{2}}\boldsymbol{C}\boldsymbol{B} & \boldsymbol{M}^{-\frac{1}{2}}\boldsymbol{A} & -\boldsymbol{M}^{-\frac{1}{2}} & 0 & 0 & 0 & 0 \\
0 & \boldsymbol{I}_{|\mathcal{V}|} & \boldsymbol{\Xi}\boldsymbol{L}_Q\boldsymbol{\Xi} & 0 & \boldsymbol{I}_{|\mathcal{V}|} & 0 & 0 \\
0 & 0 & 0 & 0 & -(\boldsymbol{\Gamma}^{\tilde{\phi}})^{\frac{1}{2}}\boldsymbol{B}\boldsymbol{C}^T & (\boldsymbol{\Gamma}^{\tilde{\phi}})^{\frac{1}{2}} & -(\boldsymbol{\Gamma}^{\tilde{\phi}})^{\frac{1}{2}} \\
0 & 0 & -(\boldsymbol{\Gamma}^{\lambda})^{\frac{1}{2}} & (\boldsymbol{\Gamma}^{\lambda})^{\frac{1}{2}}\boldsymbol{C}\boldsymbol{B} & 0 & 0 & 0 \\
0 & 0 & 0 & -(\boldsymbol{\Gamma}^{\eta})^{\frac{1}{2}} & 0 & 0 & 0 \\
0 & 0 & 0 & (\boldsymbol{\Gamma}^{\eta})^{\frac{1}{2}} & 0 & 0 & 0
\end{bmatrix} \\
&= \boldsymbol{\Gamma}\underbrace{\begin{bmatrix}
0 & -\boldsymbol{B}\boldsymbol{C}^T & 0 & 0 & 0 & 0 & 0 \\
\boldsymbol{C}\boldsymbol{B} & \boldsymbol{A} & -\boldsymbol{I}_{|\mathcal{V}|} & 0 & 0 & 0 & 0 \\
0 & \boldsymbol{I}_{|\mathcal{V}|} & \boldsymbol{\Xi}\boldsymbol{L}_Q\boldsymbol{\Xi} & 0 & \boldsymbol{I}_{|\mathcal{V}|} & 0 & 0 \\
0 & 0 & 0 & 0 & -\boldsymbol{B}\boldsymbol{C}^T & \boldsymbol{I}_{|\mathcal{E}|-|\sigma^+|} & -\boldsymbol{I}_{|\mathcal{E}|-|\sigma^-|} \\
0 & 0 & -\boldsymbol{I}_{|\mathcal{V}|} & \boldsymbol{C}\boldsymbol{B} & 0 & 0 & 0 \\
0 & 0 & 0 & -\boldsymbol{I}_{|\mathcal{E}|-|\sigma^+|} & 0 & 0 & 0 \\
0 & 0 & 0 & \boldsymbol{I}_{|\mathcal{E}|-|\sigma^-|} & 0 & 0 & 0
\end{bmatrix}}_{\boldsymbol{D}} \\
&= \boldsymbol{\Gamma}\boldsymbol{D}
\end{aligned}
\tag{28}
$$

2) σ^- is enlarged. When $\tilde{\boldsymbol{\phi}} - \overline{\boldsymbol{\theta}} < 0$, the variable $\boldsymbol{\eta}^+$ switches from zero to a positive value, which results in the removal of a positive term $(\gamma_{ij}^{\eta})^2(\tilde{\phi}_{ij} - \overline{\theta}_{ij})^2/2$ from the Lyapunov function . This leads to a discontinuity and nonincreasing in $V(\tilde{\boldsymbol{z}})$.

The change in σ^- follows the same pattern to the discussion above. Hence we claim that $V(\tilde{\boldsymbol{z}})$ is nonincreasing.

Following [11, Lem. 5], the trajectory remains in a compact set. According to the property of compact set and the fact that $V(\tilde{\boldsymbol{z}})$ is nonincreasing along the trajectory, it follows that:

$$
V^*(\tilde{\boldsymbol{z}}) = \lim_{t\to\infty} V(\tilde{\boldsymbol{z}}(t)) = \lim_{\tilde{\boldsymbol{z}}(t)\to\tilde{\boldsymbol{z}}^*} V(\tilde{\boldsymbol{z}}(t)) = V(\tilde{\boldsymbol{z}}^*) = 0 \tag{29}
$$

where $\tilde{\boldsymbol{z}}^*$ is an equilibrium that satisfies $\boldsymbol{H}(\tilde{\boldsymbol{z}}^*) = 0$.

Finally, we prove that $\boldsymbol{u}(t)$ is bounded in its power rating constraints along the entire trajectory.

Let $\hat{u}_i = \Big[u_i - \omega_i - c_i \sum_{j=1}^{n} Q_{ij}(c_i u_i - c_j u_j)\Big]_{\underline{u}_i}^{\overline{u}_i}$. Then (16c) can be rewritten as $\dot{u}_i = \hat{u}_i - u_i$. According to Laplace transform, we have

$$
\mathcal{L}\Big(u_i\Big)(s) = \frac{1}{\Big(s+1\Big)}\mathcal{L}\Big(\hat{u}_i\Big)(s).
$$

Then by applying convolution, we derive

$$
\begin{aligned}
u_i(t) = k_i\xi_i(t) &= \int_0^{\infty} \hat{u}_i(t-\tau)e^{-\tau}d\tau \\
&= \int_0^{t} \hat{u}_i(t-\tau)e^{-\tau}d\tau
\end{aligned}
$$

since $\underline{u}_i \le \hat{u}_i \le \overline{u}_i$ and according to integral inequality,

$$
\int_0^t \underline{u}_i e^{-\tau}d\tau \le u_i(t) \le \int_0^t \overline{u}_i e^{-\tau}d\tau
$$

then we have

$$
\underline{u}_i(1-e^{-t}) \le u_i(t) \le \overline{u}_i(1-e^{-t})
$$

which concludes the proof of *Theorem* 2.